A Differential Mechatronic Device: Design, Simulation and Experimental Results

[1]Alberto Borboni, [1]Francesco Aggogeri, [1]Davide Moscatelli
[1]*Università degli Studi di Brescia, DIMI, alberto.borboni@ing.unibs.it*

Abstract

Differential mechanisms are widely studied in literature, from a theoretical viewpoint and for applicative reasons. A differential mechanism is a mechanical system with one or more output motions resulting from the combination of different input motions acting on the same degree of freedom. In this work, we point the attention on planar differential systems (a monoaxis and a Cartesian device) composed by belts and pulleys. Particularly the Vernier effect is used to realize high-speed and high-accuracy devices with low-cost components. Simplified models of these two systems are presented to show the main kinematic and dynamic features. An advanced model is then realized for the Cartesian device with the aid of the Dymola software and simulation results are compared with the expected ones from the simplified model. The control of the system is realized with three PI systems (proportional-integrative) optimized via an adaptive logic. Finally early experimental results are presented only for the monoaxis system.

Keywords: *a differential mechanism, the high-accuracy Vernier effect, Dymola dynamic model, high-speed device*

1. Introduction

In literature, there are various examples of differential mechanisms, that are mechanisms with one or more output motions resulting from the combination of different input motions acting on the same degree-of-freedom (DOF). A comprehensive work is proposed by Molian [1] where compounds incorporating up to three differentials are synthesized and listed, but the method can be used for compounds of any order. Vnukov [2] from an analysis of crankshaft rolling bearings concluded that such bearings should be considered as differential mechanisms. Beletskii and Ambartsumyants [3] proposed a solution to the problem of the synthesis of a differential-lever Dwell mechanism. Sanger [4] proposed a modern approach with a matrix method in the analysis and synthesis of coupled differentials and differential mechanisms. An interesting application is described by Koreis [5] that showed different types of hydraulic wheel drive for earth moving machinery considering an automatic system for rotation difference control of hydraulic wheel drive. Kota and Bidare [6] proposed a systematic synthesis approach for multi DOF differential systems. Chen and Yao [7] suggested a topological method for the synthesis of compound geared differential mechanisms. The theoretical research produced different applicative results. Jiang, Cai and Liu [8] realized a new type of humanoid finger where a two DOF base joint is designed with a differential mechanism and distal two joints are mechanically coupled. Zhang, Dong and Lu [9] produced a passive robot intended for direct collaboration with a human operator, that implemented a five-bar architecture based on differential gears. The kinematic and dynamic models of serial robot architecture were built up in terms of different coupling modes between differential mechanisms and joints. Hernández, Bai, and Angeles [10] proposed a chain of spherical Stephenson mechanisms for a gearless pitch-roll wrist. The wrist consisted of spherical cam-rollers and spherical Stephenson linkages; two roller-carrying disks drive a combination of cams and Stephenson mechanisms rotating as a differential mechanism. Lahr and Hong [11] realized a cam-based infinitely variable transmission where a compact, lightweight, and capable differential mechanism based on a cord and pulley system is developed to double the number of followers in contact with the cam at any time, thereby reducing the contact stress between the followers and the cam surface considerably.

Basing on this literature, we are proposing a differential mechanism approach to connect two motors to the end-effector of the mechanism via an interposed differential belt pulley system that can eliminate the overconstraint associated to the presence of two actuators working on the same DOF and allows to control the output motion of the end-effector as a composition of the input motions. In this way, the

presence of speed reducers is not necessary and we can realize very high-speed controlled movements with low-cost components, due to the Vernier effect. The proposed architectures presented actuators physically connected with the frame, thus drastically reducing the effects of inertias, that can be really important in presence of high-accelerations.

2. Simplified kinematic and dynamic model

A preliminary example is represented by a monoaxis system that realizes a linear movement (Figure 1). The structure of this device is based on a differential mechanism (Burton). Referring to Figure 1, the pulleys 3 and 4 are mounted on a carriage which runs horizontally on a rectilinear guide. Other four pulleys are mounted on the bench frame: the pulleys 1 and 2 are motorized, while the pulleys 5 and 6 are free spinning. The six pulleys are interconnected by a belt.

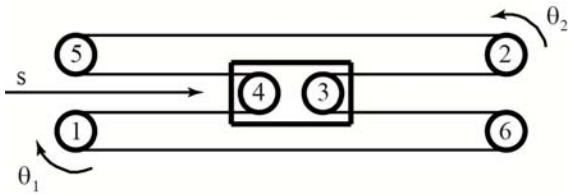

Figure 1. Structural scheme of the monoaxis system

If pulley 2 remains stationary while pulley 1 is moving, the system is nothing but a Burton mechanism, where displacement s_1 of the carriage, due to a rotation of pulley 1, is described by (1), where r_1 is the radius of the pulley 1. Similarly, if pulley 1 is stationary while pulley 2 is moving, the carriage displacement is quantified by (2), where r_2 is the radius of the pulley 2. On the other hand, if pulleys 1 and 2 are moving simultaneously, the global displacement s of the carriage is given by (3).

$$s_1 = \theta_1 r_1 / 2 \tag{1}$$

$$s_2 = \theta_2 r_2 / 2 \tag{2}$$

$$s = s_1 + s_2 = \left(\theta_1 r_1 + \theta_2 r_2\right) / 2 \tag{3}$$

The first and the second order derivatives of (3) give the carriage speed and acceleration, as shown in (4), where the dotted variables are the angular speeds and accelerations of the pulleys.

$$v = \left(\dot{\theta}_1 r_1 + \dot{\theta}_2 r_2\right) / 2, \quad a = \left(\ddot{\theta}_1 r_1 + \ddot{\theta}_2 r_2\right) / 2 \tag{4}$$

The rotations of the two motor pulleys 1 and 2 are combined by the belt to generate the linear output movement of the carriage. The use of two drivers for only one output DOF (the carriage displacement) induces a Vernier effect that increases the positioning accuracy. The Vernier effect can be explained as follows. Let's suppose, for the sake of simplicity, that the radii of the six pulleys are all equal, and that incremental encoders are used as feedback sensors on the two motors with different number of steps. In addition, always referring to Figure 1, suppose that the minimum rotation identified by the encoders is $\Delta\theta_1$ for pulley 1 and $\Delta\theta_2$ for pulley 2. Then, the minimum displacement of the carriage realized is Δs, as shown in (5), where the rotation of motor 2 is opposite to the one given in Figure 1, and $r_1 = r_2 = r$. Now, if the encoder on pulley 1 has T_1 steps and the encoder on pulley 2 has T_2 steps, as described in (6), the minimum displacement of the carriage Δs takes the form shown in (7), which is the same accuracy that could be achieved by an equivalent monoaxis system with only one encoder having a larger number of steps (8).

$$\Delta s = r\left(\Delta\theta_1 - \Delta\theta_2\right) / 2 \tag{5}$$

$$\Delta\theta_1 = 2\pi / T_1, \quad \Delta\theta_2 = 2\pi / T_2 \tag{6}$$

$$\Delta s = 2\pi r\left(T_2 - T_1\right) / \left(2T_1T_2\right) \tag{7}$$

$$T_{eq} = 2T_1T_2 / (T_2 - T_1) \tag{8}$$

The differential mechanism principle was also applied in this work to a Cartesian xy devices [12] (Figure 3). Three motors fixed on a frame lead a belt which, in turn, drive a 14 pulleys system: four of them (the three motorized pulleys and one idle) are mounted directly on the bench frame, eight pulleys are mounted on the carriage running along direction y, two pulleys are mounted on the carriage running along direction x. Assuming as positive the directions given in Figure 3 and considering that the motor pulleys have the same radius R, it is possible to show that the displacements s_x and s_y of the carriage can be described by (9).

$$s_x = R(\theta_1 - \theta_3)/2, \quad s_y = R(\theta_1 - \theta_2)/2 \tag{9}$$

In the same way as in the monoaxis system, the device has a redundant (dual) DOF, being the carriage displacement in the x and in the y direction, and a third DOF related to the idle movement of the belt on the pulleys. Consider the displacement of the carriage due to the rotation of a single motor. The carriage displaces: in straight line at 45° with a rotation θ_1; along axis y with a rotation θ_2; along axis x with a rotation θ_3. The speed and the acceleration in the directions x and y are shown in (10-11), where the dotted variables are the angular speeds and accelerations of the motors.

$$v_x = R(\dot{\theta}_1 - \dot{\theta}_3)/2, \quad v_y = R(\dot{\theta}_1 - \dot{\theta}_2)/2 \tag{10}$$

$$a_x = R(\ddot{\theta}_1 - \ddot{\theta}_3)/2, \quad a_y = R(\ddot{\theta}_1 - \ddot{\theta}_2)/2 \tag{11}$$

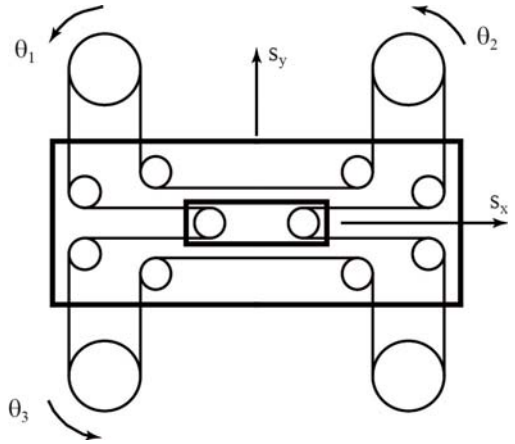

Figure 3. Structural scheme of a differential Cartesian system.

Analogously to the monoaxis case, the minimum carriage displacement can be found out along the two orthogonal directions with the equation described in (12).

$$\Delta s_x = R(\Delta\theta_1 - \Delta\theta_3)/2, \quad \Delta s_y = R(\Delta\theta_1 - \Delta\theta_2)/2 \tag{12}$$

Again, the principle based on the differential mechanism allows to achieve the Vernier effect on either sliding direction. In fact, suppose that $\Delta\theta_1$, $\Delta\theta_2$ and $\Delta\theta_3$ are finite values which depend on the resolution of the encoders mounted on the motors. Combining the movement of the three motors, it is possible to obtain a grid of positioning points much finer than the one that can be obtained with only two motors.

As an example of path planning [13], it is interesting to show the relationships between the motors speeds, in relation to the carriage movement, along straight trajectories. To execute a displacement parallel to axis x, the relation (13) is sufficient; with (14), the system can execute a displacement

parallel to the axis y; finally, with (15), the system can execute a straight displacement inclined α respect to axis x.

$$\dot{\theta}_1 = \dot{\theta}_2 \tag{13}$$

$$\dot{\theta}_1 = \dot{\theta}_3 \tag{14}$$

$$\tan\alpha = \frac{\dot{\theta}_1 - \dot{\theta}_2}{\dot{\theta}_1 - \dot{\theta}_3} \tag{15}$$

In reference to the dynamic of the system, it's possible to demonstrate that torques C_1, C_2 and C_3 (16) applied on the respective motors, aimed to generate a predefined carriage movement, being M_x and M_y respectively the integral mass at the carriage generated by the movement in direction x and the movement in direction y.

$$\begin{aligned} C_1 &= M_x\left(\ddot{\theta}_1 - \ddot{\theta}_3\right)R^2/4 + \left(M_x + M_y\right)\left(\ddot{\theta}_1 - \ddot{\theta}_2\right)R^2/4 \\ C_2 &= \left(M_x + M_y\right)\left(\ddot{\theta}_2 - \ddot{\theta}_1\right)R^2/4 \\ C_3 &= M_x\left(\ddot{\theta}_3 - \ddot{\theta}_1\right)R^2/4 \end{aligned} \tag{16}$$

Briefly, we can enumerate the main features of this kind of machine:

as it can be seen from (9-12), if the same motion is applied to all the motors (for example a unique speed constant) no displacement will be obtained at the end-effector allowing, i.e. the gripping by external devices [14, 15];

it is possible to add an angular speed signal constant (now on common rotational speed) to every motor, keeping the desired trajectory unchanged, in order to guarantee the non-inversion of the motors motion thus excluding static friction problems;

there is the possibility to combine the motion of the motors to obtain, other factors being equal, a higher dynamics;

for the Cartesian mechanism the presence of θ_1 in both expressions of (9) makes the mechanism hard to control (synchronization, drift phenomenon).

3. Advanced kinetostatic controlled model

The model of the system has been realized with an object-oriented, declarative, multi-domain modeling language used for component-oriented modeling of complex system. In particular it has been used a Modelica-based software called Dymola (DYnamic MOdel LAboratory) to carry out a dynamic model of the Cartesian differential mechanism just described in section 2.

Dynamical models are not defined using the usual ordinary differential equations (ODE) but with the more general differential algebraic equations (DAE). This peculiarity allows the user to describe the model by its own implicit equation while the input-output relation is obtained by the analytical solver within Dymola. The proposed model is shown in Figure 4. As it can be seen, the model is a collection of submodels properly linked each other and that in turn may contain other submodels and so on. Worthy of note are the submodels that follow: Motor Model; Trajectory generator; Carriage; Control.

As a note, no belt is defined, due to its representation as a discontinuous equation that is not easily implementable in Modelica. Transmission of torque and motion is granted by rotational flanges. The mechanism has a position loop closed at the central pulleys and this loop produces an error in compilation. To solve this problem the distance constraint that stands between central pulleys has been removed and substituted with a constraint to the motion of the tightening pulley (now directly linked to the motors).

The submodel of the Motor is very simple and it is represented by a pseudo-ideal speed generator with associated torque saturation and a rotational inertia.

The submodel of the Trajectory Generator is composed by two other sub-models: the set point generator and the inverse kinematics [16] of the mechanism, that respectively defines the Cartesian

values of the trajectory and expresses them in terms of rotations of the three motors. The implemented set point generator allows to define circular and straight trajectories.

The submodel of the Carriage is the most complex and contains all the submodels of the pulleys. There are two kind of pulley in this model: standard and rototranslational. A standard pulley is defined with a simple inertia that is interposed between the interfaces of the model. On the other hand, a rototranslational pulley is a quite complex model with a kinematics described by a chain of ideal components available in Dymola. The model of rototranslational pulley is shown if Figure 4 on the left. Two input flanges are present in this model to transfer onto the pulley torques coming from the other component. Ideal gear blocks allow to set the proper sign and magnitude for the torque contribution of the flanges. Three ideal rolling wheel models combine the motion reproducing the kinematic relationship that drives a rototranslational pulley.

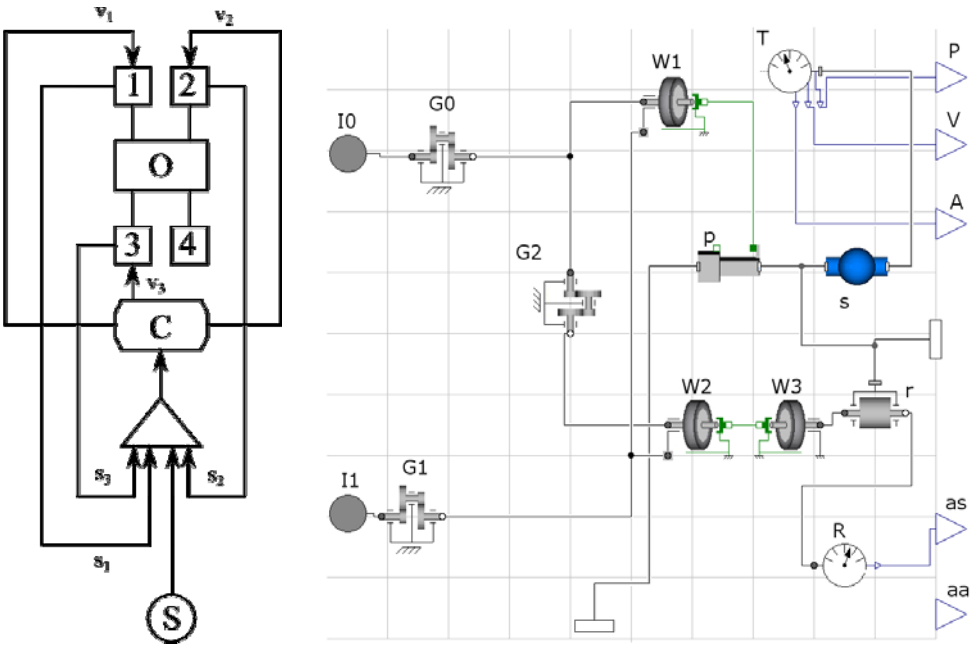

Figure 4. On the left: model of the Cartesian mechanism, where 1, 2, 3 and 4 are, respectively the first, the second, the third and the fourth pulley, O is the output motion of the carriage, C is the controller, s_i and v_i are, respectively the displacement and speed of the i^{th} pulley, S is the set-point. On the right: model of the rototranslational pulley, where I_i is the input displacement and the input torque associated to the i^{th} side of pulley, G_i is the i^{th} ideal gearbox, W_i is the i^{th} wheel that converts prismatic from/to rotary motion, p is a prismatic joint, r is the rotary inertia of the pulley, s is the inertia of the pulley, R is the angular sensor, T is the displacement sensor, p, v and a are, respectively the position, velocity and acceleration output vectors, as and aa are respectively the angular speed and acceleration outputs.

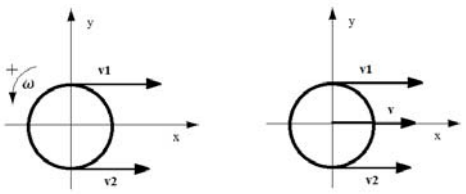

Figure 5. Kinematic scheme of the pulley.

Referring to Figure 5, the angular speed ω and the translational speed v of a pulley can be expressed (17) in terms of the input and output belt speeds v_1 and v_2.

$$\omega = (v_2 - v_1)/R, \quad v = (v_2 + v_1)/2 \tag{17}$$

With the superposition effect, the equation (10), can be used to define the v_x and v_y speeds of the carriage in terms of the $\dot{\theta}_1$, $\dot{\theta}_2$ and $\dot{\theta}_3$ rotary speeds of the pulleys. We will introduce also the common rotary speed $\dot{\theta}_0$: this quantity is set arbitrary to avoid inversions of the speed of every pulley and is summed to every pulley speed (this is to avoid different friction problems). Then, the value of $\dot{\theta}_0$ cannot be excessive to avoid fatigue of the belt. We will also introduce the coefficient of combination λ between the two motors speeds, $\dot{\theta}_1$ and $\dot{\theta}_2$, thus the expression (10) takes the form shown in (18), where the red term is obtained stopping the pulleys 2 and 3, the blue term is obtained stopping the pulleys 1 and 3, the orange term is obtained stopping the pulleys 1 and 2, and the green term is obtained when all the pulleys have the same speed $\dot{\theta}_0$. The coefficient of combination λ is set in the model to determine indirectly the angular speeds $\dot{\theta}_1$ and $\dot{\theta}_2$ of the associated pulleys.

$$v_y = R\left[\lambda\left(\dot{\theta}_1 + \dot{\theta}_0\right) - (1-\lambda)\left(\dot{\theta}_2 + \dot{\theta}_0\right)\right]/2, \quad v_x = R\left[\left(\dot{\theta}_1 + \dot{\theta}_0\right) - \left(\dot{\theta}_3 + \dot{\theta}_0\right)\right]/2 \tag{18}$$

The control model simply contains three PI (proportional-integrative) position control loops [17], one for each motor; because the forecasted dynamics of the machine is slow and, eventually, an evolution of this type of control will implement a feed-forward strategy. The definition of control parameters, such as the proportional gain (k_p) and the integral time (t_i) was performed through a simulation. Then, an adaptive optimization has been executed based upon the minimization of two figures of merit, as shown in section 5.

4. Simulation results

The simulation was performed on a standard circular trajectory centered in the point C (-25, 0) [mm], with a diameter of 50 mm, a target speed v equal to 5 mm/s, a common rotary speed ω_0 equal to 2.5 rad /s and a coefficient of combination λ between the two motors speeds, ω_1 and ω_2, acting on the same DOF equal to 0.5 (18), v is the speed of the carriage.

Once defined the motors inputs (Figure 6), the simulation can be carried out and a number of results and information can be obtained. For our purpose we focused on kinematical and dynamical data such as: the trajectory of the end-effector and the torque required to the motors.

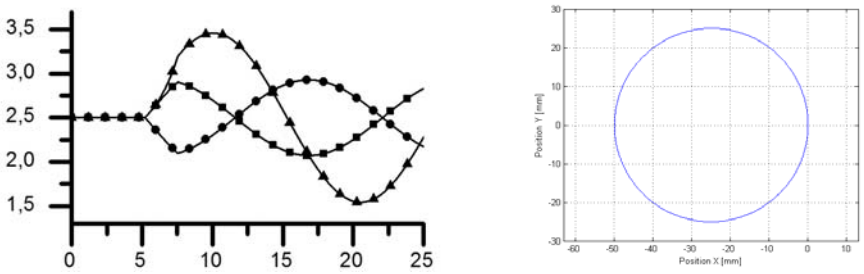

Figure 6. On the left: motor input speeds [rad/s] versus time [s], where squares are ω_1, circles are ω_2, triangles are ω_3. On the right: simulated trajectory in the plane [mm].

The simulated trajectory is shown on the right side of Figure 6 and, as it can be seen, the model is able to realize the desired target (a circular trajectory) respecting the kinematic architecture of the mechanism. Motor torques are shown in Figure 7 and there are some differences between theoretical

and simulated results, due to the difference between the advanced DAE model and the theoretical model.

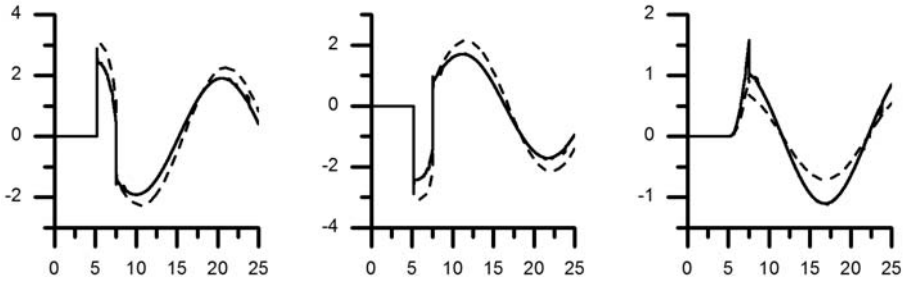

Figure 7. Theoretical (broken line) and simulated (continuous line) torques [N mm] versus time [s] for the first (on the left) motor, for the second motor (center) and for the third motor (on the right).

The differences between the theoretical and the simulated torques can be associated to:

- Asymmetry introduced by the DOF introduced between the central pulleys. It could be useful consider cumulative values of motors mechanical action;
- The DAE model takes account of the inertial component of each motor and each pulley which is not considered in theoretical expression;
- Motors have torque saturation in DAE model and that introduces an unforeseen delay in the system;
- Drift errors may occur due to solver discretization.

5. Optimization and adaptive control

An adaptive logic [18-20] has been adopted to select properly the control parameters, with the aim of respecting the desired kinematical behavior. More in detail, two figures of merit have been chosen, ITAE (Integral of Time multiplied by Absolute Error) and ISTE (Integral Square Time Error) to be minimized, as shown in (19), where t is the time and e(t) is the position temporal error measured directly on the three motors.

$$ITAE = \int t\left|e(t)\right|dt, \quad ISTE = \int t^2 e^2(t)\,dt \tag{19}$$

Then an hybrid adaptive genetic algorithm [21-23] was implemented to minimize three output figures of merit contemporaneously (one for each motor), changing iteratively the normalized values of two input parameters of the PI controller, the proportional gain k_p and integral time t_i, and an input parameter associated with the optimization algorithm itself γ_1 that is the adaptive coefficient that manages the tradeoff between an aggressive strategy and a conservative one, as shown in (20). γ_1 is used to correct the input value at each iteration, realizing a hybrid algorithm able to rapidly accelerate the convergence process. As a matter of fact γ_1 is suggested to be between 0 and 1 and, when the absolute value of γ_1 is high, the parameters are subjected to a high change at every iteration. This behavior can ideally allow to gain the optimal value rapidly but increments the risk of instability and of divergence of the optimization algorithm.

$$k_P(i+1) = k_P(i) + \gamma_1 \cdot ITAE, \quad t_i(i+1) = t_i(i) - \gamma_1 \cdot ISTE \tag{20}$$

After different evaluations in the selection of various figures of merit, ITAE [24] was adopted for k_p adaptation because the proportional component should be increased if the absolute error is high, especially with the increase of time t, whereas ISTE [25] was used for integral action t_i because it penalizes more errors at high time (i.e. close to the setpoint value) and, in this way, it is expected to reduce oscillations around the steady state conditions.

Figure 8 shows the evolution of the ITAE and ISTE errors computed on the first motor during the evolution.

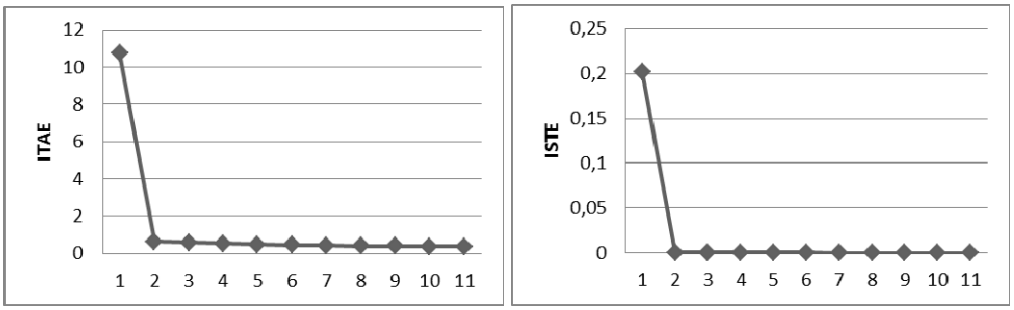

Figure 8. Evolution of the ITAE and ISTE errors on the first motor versus the iteration number of the optimization algorithm

6. Experimental results

We realized a monoaxis system that can gain an important accuracy with two low-resolution encoders at high speed with the Vernier effect, with the previously described differential kinematic structure.

As an example, a carriage moved at 10 m/s by pulleys having a radius equals to 20 mm, can be positioned with a theoretical accuracy of 0.001 mm with low-cost components such as two commercial encoders with 1000 and 1024 steps, a gate array with 85 kHz sampling frequency, and two motors with a maximum speed of 5000 rev/min. Moreover, the fact that the same carriage displacement can be obtained by different combinations of the motors rotations, further enhances the trajectory planning. In fact, it will be possible to choose those particular motion profiles that, while positioning the carriage with high accuracy, optimize other motion parameters or the dynamic behavior of the system. To make a curious example, the numerator of formula (4) on the left side can be made equal to zero with proper opposite values for the motors angular speed: so the carriage can be kept still with the two motor running.

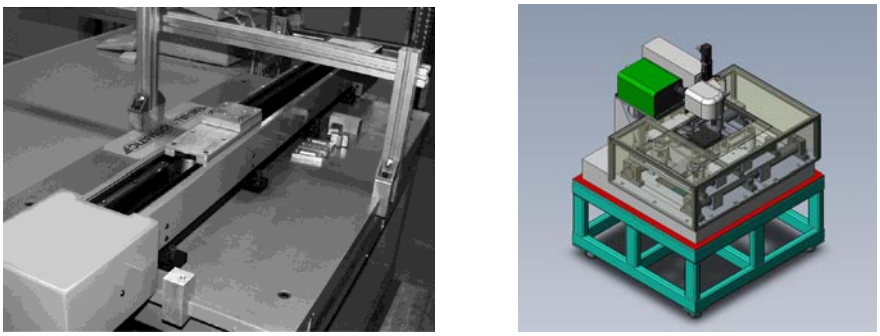

Figure 9. The monoaxis system (left) and Cartesian system (right).

A prototype of the monoaxis system (Figure 9), based on the working principle previously described, has already been built. The monoaxis system comprises the following devices as main components: two motors having a nominal torque of 1.8 Nm and a peak torque of 7.2 Nm; moment of inertia, including the shaft and the motor pulleys, is approximately 3 10^{-4} kg m^2; a metallic belt connecting six pulleys, each one having radius 20 mm and a moment of inertia of nearly 10^{-4} kg m^2; 1024 step encoders; a carriage of approximately 3 kg, which runs on wheels along a rectilinear guide for a max displacement of 1 m; a programmable controller on two axes with a 100 kHz gate array.

The measured performance obtained in a continuous cyclical movement have been: maximum carriage speed is 9.2 m/s; maximum carriage acceleration is 102 m/s^2; position repeatability at the ends of the stroke is 3.7 μm.

Different experimental test were performed on the system, i.e. in Fig. 10, are shown an evaluation of the stiffness with a response to a step force (Fig. 10 on the left), the friction force of the system (Fig 10 in the middle) and the effects of backlash in terms of acceleration (Fig. 10 on the right).

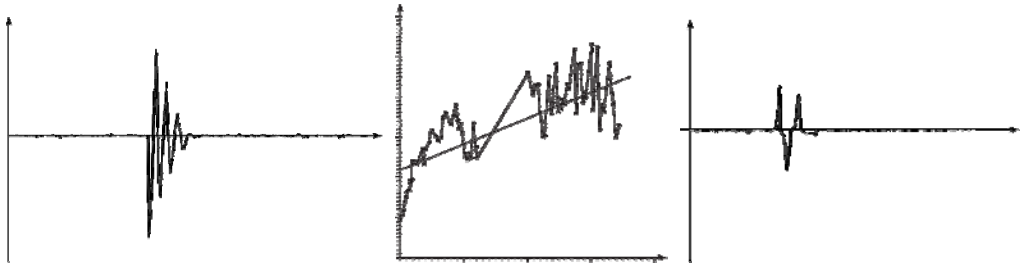

Figure 10. Response to a step force: acceleration versus time (left); friction force versus speed (middle); acceleration versus time in presence of backlash (right).

We are working also on a prototype of the Cartesian system (Figure 9) and further experimental results will be available in the next future. Especially we would consider also the presence of elastic elements and compliances in general [26, 27], that will be properly compensated through adequate techniques [28].

7. Conclusions

The proposed differential architectures can be easily modeled with rigid body models, but a more precise modeling approach, with lumped parameters and a DAE formulations, exhibits a more realistic behavior than can facilitate an accurate design of the machine and, especially of the controller. As a matter of fact this model allows us to test different control systems in a simulated environment with different iterative algorithms. This quantitative result accelerated the design and realization process of the machines, that exhibit an accurate positioning with high speeds. Future activities will involve a sensitive or a stochastic [23, 29, 30] analysis of the process to evaluate its robustness and its evaluation within a complete production system [29].

8. References

[1] Molian S., "Kinematics of compound differential mechanisms", Proc (Part 1) Inst Mech Eng, pp. 733-739, 1972.

[2] Vnukov V.P., "Kinematic Calculation of a Rolling Bearing on a Connecting-Rod", Russian Engineering Journal, vol **53**, no 5 pp. 25-7, 1973.

[3] Beletskii V.Y. and Ambartsumyants R.V., "Differential-Lever Dwell-Type Mechanism", Russian Engineering Journal, vol **53**, no 6, pp. 34-37, 1973.

[4] Sanger D.J., "Matrix Methods in the Analysis and Synthesis of Coupled Differentials and Differential Mechanisms", 4th World Congr on the Theory of Mach and Mech, pp. 27-31, 1975.

[5] Koreis J., "Automatic differential mechanism of hydraulic wheel drive", Sterowanie & Naped. Hydraul., vol **2**, pp. 17-20, 1987.

[6] Kota S. and Bidare S., "Systematic synthesis and applications of novel multi-degree-of-freedom differential systems", in 22nd Biennial ASME Mechanisms Conference, pp. 235-242, 1992.

[7] Chen D.Z. and Yao K.L., "Topological synthesis of compound geared differential mechanisms", International Journal of Vehicle Design, vol **31**, no 4, pp. 427-439, 2003.

[8] Jiang L., Cai H., and Liu H., "New type integration humanoid finger and its dynamics analysis", Jixie Gongcheng Xuebao/Chinese Journal of Mechanical Engineering, vol **40**, no 4, pp. 139-143+148, 2004.

[9] Zhang L.X., Dong Y.H., and Lu D.M., "Research on kinematics and dynamics of five-bar Cobot", Harbin Gongcheng Daxue Xuebao/Journal of Harbin Engineering University, vol **25**, no 3, pp. 337-340, 2004.

[10] Hernández S., Bai S.P., and Angeles J., "The design of a chain of spherical stephenson mechanisms for a gearless pitch-roll wrist", in ASME Design Engineering Technical Conferences and Computers and Information in Engineering Conference, pp. 1129-1138, 2004.
[11] Lahr D.F. and Hong D.W., "Contact stress reduction mechanisms for the cam-based infinitely variable transmission", in 31st ASME Mechanisms and Robotics Conference, pp. 449-456, 2008.
[12] Mistikoglu S. and Özyalçin I., "Design and development of a cartesian robot for multi-disciplinary engineering education", International Journal of Engineering Education, vol **26**, no 1, pp. 30-39, 2010.
[13] Cui Y., "Mobile robot path planning in dynamic environment based on genetic algorithm", International Journal of Digital Content Technology and its Applications, vol **6**, no 18, pp. 130-138, 2012.
[14] Borboni A., Aggogeri, F.; Faglia, R., "Design and Analysis of a Fibre-Shaped Micro-Actuator for Robotic Gripping", International Journal of Advanced Robotic Systems, vol **10**, no 149, pp. 1-10, 2013.
[15] Aggogeri F., Al-Bender F., Brunner B., Elsaid M., Mazzola M., Merlo A., Ricciardi D., De La O Rodriguez M., and Salvi E., "Design of piezo-based AVC system for machine tool applications", Mechanical Systems and Signal Processing, vol **36**, no 1, pp. 53-65, 2013.
[16] Borboni A., "Solution of the inverse kinematic problem of a serial manipulator by a fuzzy algorithm", pp. 336-339, 2001.
[17] Matušů R. and Prokop R., "A Matlab program for single-parameter tuning of PI controllers", International Journal of Mathematics and Computers in Simulation, vol **7**, no 1, pp. 77-84, 2013.
[18] Huang D., Wu Z., Mo H., and Zhang Y., "Optimization for PID control parameters tuning by using second-order particle swarm optimization based on dynamic adaptive", International Journal of Advancements in Computing Technology, vol **5**, no 5, pp. 56-63, 2013.
[19] Shen Y., "Research of robot path planning", International Journal of Advancements in Computing Technology, vol **5**, no 5, pp. 298-304, 2013.
[20] Zhang Y., "Research of spatial layout optimization based on genetic algorithm", International Journal of Advancements in Computing Technology, vol **5**, no 5, pp. 321-329, 2013.
[21] Borboni A., Bussola R., Faglia R., Magnani P.L., and Menegolo A., "Movement optimization of a redundant serial robot for high-quality pipe cutting", Journal of Mechanical Design, Transactions of the ASME, vol **130**, no 8, pp. 0823011-0823016, 2008.
[22] Antonini M., Borboni A., Bussola R., and Faglia R., "Automatic procedures as help for optimal cam design", in Proceedings of 8th Biennial ASME Conference on Engineering Systems Design and Analysis, 2006.
[23] Antonini M., Borboni A., Bussola R., and Faglia R., "A genetic algorithm as support in the movement optimisation of a redundant serial robot", in Proceedings of 8th Biennial ASME Conference on Engineering Systems Design and Analysis, 2006.
[24] Nowacka-Leverton A. and Bartoszewicz A., "ITAE optimal variable structure control of second order systems with input signal and velocity constraints", Kybernetes, vol **38**, no 7, pp. 1093-1105, 2009.
[25] Wang H., Li X.M., Yan W., and Huang M.H., "A novel AQM algorithm based on the PI controller with minimum ISTE", Jisuanji Xuebao/Chinese Journal of Computers, vol **35**, no 5, pp. 951-963, 2012.
[26] Amici C., Borboni A., Faglia R., Fausti D., and Magnani P.L., "A parallel compliant meso-manipulator for finger rehabilitation treatments: Kinematic and dynamic analysis", in IEEE/RSJ International Conference on Intelligent Robots and Systems, pp. 735-740, 2008.
[27] Bonnemains T., Chanal H., Bouzgarrou B.C., and Ray P., "Dynamic model of an overconstrained PKM with compliances: The Tripteor X7", Robotics and Computer-Integrated Manufacturing, vol **29**, no 1, pp. 180-191, 2013.
[28] Ermilov A.S. and Ermilova T.V., "Synthesis of an active compensation algorithm for elastic oscillations with nonstationary parameters for deformable spacecrafts", Automation and Remote Control, vol **73**, no 4, pp. 652-664, 2012.
[29] Aggogeri F., Mazzola M., Borboni A., and Faglia R., "A novel logic and approach to speed up simulation and analysis of production systems", Journal of Convergence Information Technology, vol **8**, no 3, 2013.
[30] Hagiwara I., Fujiwara T., and Nagabuchi K., "Optimum Analysis for Structural Vibration Character (First Report Proposition of a New Eigen Mode Sensitive Analysis and Comparison Between Some Different Methods)", Nippon Kikai Gakkai Ronbunshu, C Hen/Transactions of the Japan Society of Mechanical Engineers, Part C, vol **52**, no 482, pp. 2607-2614, 1986.